Effect of Surface Adhesion on the Rough Contact Response Near Complete Contact

Siyuan ZHANG*, Yanwei LIU**

*School of Mechanical Engineering, University of Shanghai for Science and Technology, Shanghai, 200093, China, E–mail: zhangsiyuan@usst.edu.cn
**Department of Mechanics and Engineering Science, College of Engineering, BIC-ESAT, Peking University, Beijing 100871, PR China, E–mail: yanwei-liu@pku.edu.cn (Corresponding author)

Nomenclature

a_{ctc} – contact radius of a single asperity; A_n – expansion coefficient; A_{nom} – nominal contact area; A_{ctc} – contact area of a single asperity; A_s - contact area of a single asperity considering adhesion; d – loading displacement; d_s – real loading displacement considering adhesion; E^* – equivalent Young's modulus; F_{ad} – adhesive force; F_s – contact force of a single asperity considering adhesion; F_{ctc} - contact force of a single asperity; h - height of a single sinusoidal-shaped asperity; $\bar{h}$ – average height of asperities; n – expansion order; N – total asperity number; R – radius of asperity summits; U – elastic strain energy; v – Poisson's ratio; w – half-width of a single asperity; z – asperity height; γ – surface energy; β – surface roughness, $\sigma / \bar{h}$; δ – deformation of a single asperity; λ – width of a single sinusoidal asperity; σ – standard deviation.

1. Introduction

The adhesive contact problems between solids are important in mechanical and biological fields, such as Micro-Electro-Mechanical Systems (MEMS) [1, 2], cell adhesion, adhesive pads of animal feet [3 – 5], etc. The accurate solution of adhesive contact can provide theoretical basis for designing wall-climbing robots and super adhesive materials. Since the adhesive effect plays an important role in microscale contact problems, it is challenging and critical to develop traditional adhesion models and propose proper adhesive models between elastic solids. The basic adhesion theories, i.e., JKR theory [6], DMT theory [7, 8] and tabor theory [9] use rigid sphere and soft elastic substrate to determine the adhesion effect.

By far, one of the best-known theories for adhesion is JKR theory, which has been developed for many different types of contacts. JKR discussed the contact between an elastic sphere with radius R and a rigid plane: the attraction force between the two objects (van der Waals forces) forms a neck when the elastic sphere comes into contact with a smooth surface, and the corresponding adhesion force can be calculated by a simple expression. In research and engineering, JKR theory is more commonly used to describe adhesive contacts because it predicts adhesion relatively well, even in the scope of DMT theory. However, the JKR model assumes that the rigid indenter is spherical and the overall deformation is assumed to be small enough, which limits its application in surface analysis of high loading condition and complex surface topography.

On the one hand, in terms of loading conditions, adhesion response of spherical asperities (JKR theory) is predicted according to Hertz solution, which is based on small strain assumptions. For example, Ciavarella [10] suggested a simple closed form solution to the adhesive contact problem under JKR regime. Prokopovich et al [11] proposed the application range of JKR theory by comparing the theoretical and experimental results, which provides the application range of JKR theory. Similar JKR-based models also include the refined adhesive model proposed by Hui et al [12], which provides a continuum mechanics approach to solve this adhesive problem. The above JKR-based methods restricted the loading conditions to small strain conditions. According to the original JKR theory, the loading process is assumed to be predicted by Hertzian solution, and then it is unloaded at the constant contact area. However, the Hertzian solution itself is not valid for high contact pressure, which will influence the unloading process when considering adhesion effect. As a result, the exact adhesive effect should be determined according to an improved analytical solution for the mechanical behaviors of a single indentation model. Therefore, it is necessary to propose a new analytical solution for rigid indenters in contact with an elastic half-space substrate which is still valid for high load conditions, especially for near complete contact.

On the other hand, since the surface morphology is determined by the shape of single indenter and the surface roughness parameters, the adhesion and contact response are very sensitive to these two quantities. Many theories have been proposed to investigate the adhesion effect between surfaces: some based on single asperity, while others based on multi-asperities, such as contact between rough surfaces [15]. So, it is critical to investigate the influence of indenter profiles and roughness parameters of rough surface on adhesion. For example, despite the JKR-related spherical indenter [13], one-dimensional wavy surface [14], elliptical-shaped asperity [15], cylinder asperity [16], and the comparison of different profiles [17] have been studied in detail. However, although spherical indenters are widely used in the study of adhesive contact, rough surface profile measurements [18] clearly show that a sinusoidal description is much more realistic than a circular asperity geometry, but the rigorous treatment of adhesive contact for three-dimensional sinusoidal indenter is still lack of investigation. In addition to the commonly used

spherical and sinusoidal-shaped indenter, the cone shape [19] is especially suitable for measuring the mechanical properties of soft materials in nano-indentation experiments [20]. By far, few studies paid attention to the adhesion response of single sinusoidal, cone shaped indenter, and rough surface analysis considering the influence of indenter shape under high loading conditions. In addition, some attempts have also been recently made to estimate the effect of adhesion between elastic rough solids with roughness following Gaussian distribution [21] and fractal dimensions [10, 22]. However, the relationship between surface roughness and adhesion effect is still an open topic. Since the characteristics of surface roughness are composed of two random parameters: indenter shape and height distribution, it is necessary to accurately describe the geometric properties and adhesive behavior of different shape indenters, which can capture the effect of roughness caused by roughness itself on contact and adhesion.

Considering the problems in current researches, in this paper, we establish an analytical adhesive model for indentation problems, and propose a discrete rough surface model. What should be emphasized is that our model greatly improves the prediction accuracy of contact relationship under high loading conditions, which provides a different perspective of characterizing and analysing the mechanical properties for rough surface. The paper is organized as follows: in Section 2, we derive the analytical solutions for spherical indenter, sinusoidal indenter and cone-shaped indenter in contact with a soft elastic half-space, and especially focus on the contact relationship under high contact pressure. Based on the analytical results in Section 2, the adhesion effect is considered in the frame of JKR theory, and a comparison of the predictions of adhesion model with different shapes is presented in Section 3. Then, a new discrete model considering adhesion for rough surface is proposed in Section 4, and the influence of surface properties (surface roughness and surface energy) to the contact responses has been discussed. Finally, we summarize our results in Section 5. Although the classical Hertz model can describe the contact response between solids under the assumption of small deformation, it ignores the influence of adhesive force, and the adhesive effect plays an important role in micro scale contact problems. Our model improves the accuracy of traditional contact model and JKR adhesive model, and provides theoretical basis for the design of adhesion biomimetic materials and MEMS systems.

2. Elastic response of rigid indenters with different profiles in contact with a soft elastic substrate

2.1. Model description

Different shapes of asperities could have the same equivalent curvature radius but they may have different mechanical properties. In this section, we consider elastic contact responses of various profiles of indenters, but the main attention is paid to accurate solutions for high contact pressure. For a single asperity, when the ratio of the indentation depth and the asperity height is close to 1, we term it as "near complete contact". We do not use the contact area fraction to define a complete contact because the substrate surface will be depressed significantly under high loading

conditions, and the contact area predicted by the theoretical solution will be deviated from the real situation.
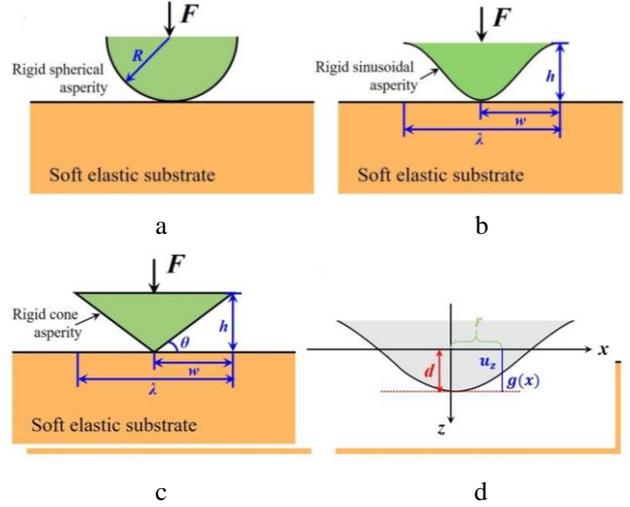
Fig. 1 Schematic of the contact model between different profiles of indenters and a soft elastic substrate: a) rigid spherical indenter; b) rigid sinusoidal indenter; c) rigid cone-shaped indenter; d) coordinate system and contact region geometry

Let us consider an elastic contact between a rigid indenter with different geometry profiles in contact with an elastic half-space, as shown in Fig. 1. The radius of curvature at the tip of the sinusoidal indenter in Fig. 1b is the same as the radius of the spherical indenter in Fig. 1a. The value of h/w for the sinusoidal indenter in Fig. 1b is the same as the tangential value $tan(\theta)$ of the cone-shaped indenter in Fig. 1c. For this contact problem, the geometric relationship of the contact region and the coordinate system diagram are shown in Fig. 1d. For the point on the rigid indenter where the radial distance is r, the total loading displacement d can be divided into two parts:

$$d = u_z + g(x), \qquad (1)$$

where: the indentation depth of the point on the surface is u_z, and the gap between the rigid indenter and the horizontal line is denoted as $g(x)$.

2.2. Analytical solution

In order to obtain the elastic response of a soft elastic substrate indented by a rigid spherical/sinusoidal asperity, the indenter profile can be described by $z(x)$, which has the following form (Eq. (2) for spherical indenter and Eq. (3) for sinusoidal indenter):

$$z(x) = \sqrt{R^2 - x^2}, \qquad (2)$$

$$z(x) = \frac{1}{2} h \left[cos\left(\frac{\pi}{w} x\right) + 1 \right], \qquad (3)$$

where: R represents the spherical radius; h and w represent the height and half-width of the asperity respectively, as shown in Figs. 1a, 1b.

According to Eq. (1), when the total loading displacement is fixed, the accurate expression of $g(x)$ directly affects the accuracy of u_z. For the axisymmetric case, the

distance $g(x)$ can be approximated through a Taylor expansion in form of $\sum A_n x^2$ where n is the order of the expansion and A_n is the expansion coefficient (for more details, see Ref. [24]). The exact distance between the initial position of the rigid spherical/sinusoidal indenter and the elastic substrate can also be written in the form of Taylor expansion, which is given by:

$$g(x) = A_1 x^2 + A_2 x^4 + A_3 x^6 + \ldots + A_n x^{2n}, \tag{4}$$

where: $A_1 = \dfrac{1}{2R}, A_2 = \dfrac{1}{8R^3}, \ldots$ for spherical indenter, and

$A_1 = \dfrac{1}{4} h(\dfrac{\pi}{w})^2, A_2 = -\dfrac{1}{48} h(\dfrac{\pi}{w})^4, \ldots$ for sinusoidal indenter.

According to Johnson and Steuermann [23], in axisymmetric case, the contact force and the compression for a single asperity can be obtained through (Eqs. (5.20), (5.21) and (5.22) in Ref. [23]):

$$F = \frac{4 A_n E^* n a^{2n+1}}{(2n+1)} \frac{2 \times 4 \times \cdots \times 2n}{1 \times 3 \times \cdots \times (2n-1)}, \tag{5}$$

$$d = \frac{2 \times 4 \times \cdots \times 2n}{1 \times 3 \times \cdots \times (2n-1)} A_n a^{2n}. \tag{6}$$

Note that when the expansion order $n = 1$, the solution for spherical indenter is essentially the classical Hertz solution $(F_{ctc} = \frac{4}{3} E^* R^{\frac{1}{2}} d)$. For sinusoidal indenter, if one substitutes the equivalent curvature $R = \dfrac{2w^2}{\pi^2 h}$ into Hertz solution, the corresponding solution is essentially the classical Hertz solution as well. For small strain loading conditions, Hertz solution is simple in form and easy to use. In fact, small deformation is very difficult to control in the experiments, so it is necessary to use an analytical solution which is still suitable for high loading conditions.

According to Eqs. (1 – 6), the contact force and contact area can be obtained under the given load. For $n = 2$, the contact response for spherical indenter has the form:

$$F_{ctc} = \frac{4E^*}{3R} \left[-\frac{3}{2} R^2 + \frac{1}{2}\sqrt{9R^4 + 12R^3 d} \right]^{\frac{3}{2}} +$$
$$+ \frac{8E^*}{15R^3} \left[-\frac{3}{2} R^2 + \frac{1}{2}\sqrt{9R^4 + 12R^3 d} \right]^{\frac{5}{2}}, \tag{7}$$

$$A_{ctc} = \pi a^2 = \pi \left[-\frac{3}{2} R^2 + \frac{1}{2}\sqrt{9R^4 + 12R^3 d} \right], \tag{8}$$

where: F_{ctc} and A_{ctc} represent the contact force and contact area of this indentation model. The loading displacement is denoted as d, and E^* represents the equivalent Young's modulus, defined as: $\dfrac{1}{E^*} = \dfrac{1-v_1^2}{E_1} + \dfrac{1-v_2^2}{E_2}$, where E_1, E_2 and v_1, v_2 are Young's moduli and Poisson ratios of the two contacting materials, respectively.

Similarly, for sinusoidal indenter, the contact response can be obtained:

$$F_{ctc} = 2\sqrt{6} E^* \frac{h\lambda}{\pi} \left(\frac{3}{4} - \sqrt{\frac{9}{16} - \frac{1}{2}\frac{d}{h}} \right)^{\frac{3}{2}} -$$
$$- \frac{8}{5}\sqrt{6} E^* \frac{h\lambda}{\pi} \left(\frac{3}{4} - \sqrt{\frac{9}{16} - \frac{1}{2}\frac{d}{h}} \right)^{\frac{5}{2}}, \tag{9}$$

$$A_{ctc} = \frac{3\lambda^2}{2\pi} \left(\frac{3}{4} - \sqrt{\frac{9}{16} - \frac{1}{2}\frac{d}{h}} \right), \tag{10}$$

where $\lambda = 2w$, representing the width of the sinusoidal indenter. From now on, we term Eqs. (7 – 10) as "extended Hertz solution".

Different from the flattening problem, the substrate deformation away from the contact zone can be neglected for present model. With the increasing deformation, using the radius of curvature at the asperity tip is not adequate, so the Hertz solution deviates from the results of extended Hertz solution, which indicates that it is only valid for very small load. However, most JKR-based adhesion model use Hertz solution to describe the non-adhesive contact behaviours, which will cause deviation at high loading conditions.

It should be noted that the accurate solution of conical indenter is different from the former method because the Steuermann solution is only valid for non-conforming surfaces, which means the initial separation between such surfaces in the contact region can be represented to an adequate approximation by a second-order polynomial. Therefore, it cannot be used for cone-shaped indentation problem. According to Popov [25, 26], the contact response of rigid cone-shaped indenter can be solved according to dimensionality reduction method, which can be expressed as (for more details, see Appendix):

$$F_{ctc} = \frac{2}{\pi} E^* \frac{d^2}{tan\theta}, \tag{11}$$

$$A_{ctc} = \frac{4d^2}{\pi tan^2\theta}, \tag{12}$$

where: $tan(\theta) = h / w$.

3. Adhesive contact between rigid indenters with different profiles and a soft elastic substrate

3.1. Basic theory

The following analysis shows how to consider adhesion in terms of extended-Hertz solution. The total potential energy of the system is composed of three parts: elastic strain energy, surface energy and potential energy of the applied force. The entire loading process can be divided into two steps, as shown in Fig. 2.

a) If adhesive force is not taken into consideration, the load can be determined according to Hertz solution when the contact area is a given value, which is the load path OA as in the original JKR paper [6]. However, as discussed in Section 2, if using Hertz solution to predict

adhesion effect, deviation will increase with the load increasing. Therefore, the actual loading curve (path OA in Fig. 2) is calculated according to Eqs. (7 – 10) in Section 2.

b) Remain the contact area A_{ctc} to be constant, rigid-body displacement will happen (this is load path AB as in the original JKR paper [6]). This displacement is unknown, but we can find its value by a minimization procedure of the total potential, as the classical Griffith crack problem. However, since the predicting deviation for contact response exists, especially for contact area versus loading displacement, using Hertz-based JKR prediction will cause deviation for indentation problem at high load. Therefore, the actual unloading curve (path AB in Fig. 2) is also based on the analytical solutions in Section 2.
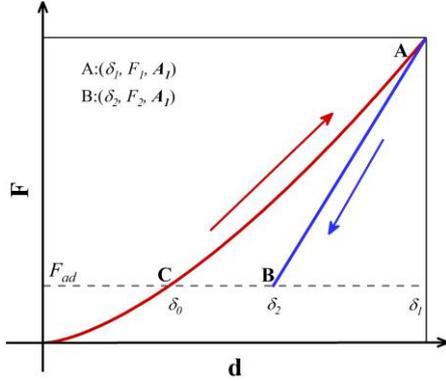
Fig. 2 Loading curve: a) load path OA obeys analytical prediction in Sec. 2; b) rigid-body displacement when the contact area remains unchanged. The values of displacement, force, and contact area at Point A and B are shown in the legend

In this section, we treat this process according to the present analytical solution for different profiles of indenters, which is not just for the spherical Hertzian contact as in the original JKR paper. During step b), since the contact area remains constant, the load decreases linearly (path AB in Fig. 2), so the linear equation of path AB can be expressed by:

$$F_2 - F_1 = \left(\frac{\partial F_{ctc}}{\partial d} \right)_{\delta_1} \cdot (\delta_2 - \delta_1), \tag{13}$$

where: δ_2 is an unknown value; $(\partial F_{ctc}/\partial d)_{\delta_1}$ represents the slope of line AB, and $(\partial F_{ctc}/\partial d)_{\delta_1} (\delta_2 - \delta_1)$ is the term for adhesion force.

During step a), the elastic strain energy can be obtained by integrating the load-displacement curve:

$$U_1(\delta_1) = \int_0^{\delta_1} F_{ctc}(\delta) d\delta, \tag{14}$$

where: $F_{ctc}(\delta)$ can be calculated by the analytical predictions in Section 2 (Eqs. (7), (9) and (11)), and δ represents the variable of displacement. For point A, the elastic strain energy is denoted by U_1, and the loading displacement is denoted by δ_1.

The loading displacement during the unloading process is unknown, which is downloading to $\delta = \delta_2$, and the elastic strain energy becomes:

$$U_2 = \int_{\delta_1}^{\delta_2} F_2(\delta) d\delta, \tag{15}$$

where: $F_2(\delta)$ is unknown, and U_2 represents the elastic strain energy of point B in Fig. 2.

The total elastic strain energy can be obtained:

$$U_e = U_1 - U_2. \tag{16}$$

If the energy per unit contact area is denoted as γ, the surface energy becomes $- \gamma A_s$, so the total potential energy U_t is:

$$U_t = U_e - \gamma A_{ctc}, \tag{17}$$

where: U_e can be obtained by Eq. (16) and A_{ctc} represents the contact area, which can be obtained according to Section 2 (Eqs. (8), (10), and (12)).

At point B in Fig. 2, the system is in a critical equilibrium state. The equilibrium position is then determined by the condition:

$$\frac{\partial U_t}{\partial A_s} = 0. \tag{18}$$

According to the chain's rule, the total potential energy can be rewritten as:

$$\frac{\partial U_e}{\partial \delta_1} \frac{\partial \delta_1}{\partial A_{ctc}} = \gamma. \tag{19}$$

Based on the approximate method proposed by Ciavarella [10], the final displacement has the form (which is Eq. (10) in Ref. [10],):

$$\delta_2 = \delta_1 - \sqrt{2\gamma \frac{\partial A_{ctc}}{\partial \delta_1} / \frac{\partial^2 F_{ctc}}{\partial \delta_1^2}}. \tag{20}$$

In this way, the adhesion force F_{ad}, real contact force F_s, and the real loading displacement d_s for the indentation model can be extended:

$$F_{ad} = -\frac{\partial F_{ctc}}{\partial d} \sqrt{2\gamma \cdot \left(\frac{\partial A_{ctc}}{\partial d} / \frac{\partial^2 F_{ctc}}{\partial d^2} \right)}, \tag{21}$$

$$F_s = F_{ctc} - \frac{\partial F_{ctc}}{\partial d} \sqrt{2\gamma \cdot \left(\frac{\partial A_{ctc}}{\partial d} / \frac{\partial^2 F_{ctc}}{\partial d^2} \right)}, \tag{22}$$

$$d_s = d - \sqrt{2\gamma \cdot \left(\frac{\partial A_{ctc}}{\partial d} / \frac{\partial^2 F_{ctc}}{\partial d^2} \right)}. \tag{23}$$

3.2. Analytical adhesive solution for asperities with different profiles

3.2.1. Rigid spherical indenter

Based on the proposed solutions for spherical asperity (Eqs. (7) and (8)), the adhesion force can be derived according to the general method of Section 3.1. Take the

first and second derivative of contact radius a_{ctc} over loading displacement, that is:

$$\frac{\partial a_{ctc}}{\partial d} = \frac{3}{2} R^3 \left(-\frac{3}{2} R^2 + \frac{1}{2} \sqrt{9R^4 + 12R^3 d} \right)^{-\frac{1}{2}} \times \left(9R^4 + 12R^3 d \right)^{-\frac{1}{2}}, \tag{24}$$

$$\frac{\partial^2 a_{ctc}}{\partial d^2} = \left(-\frac{9}{4} R^6 \right) \times \left(-\frac{3}{2} R^2 + \frac{1}{2} \sqrt{9R^4 + 12R^3 d} \right)^{-\frac{3}{2}} \times (9R^4 + 12R^3 d)^{-1} + (-9R^6) \times$$

$$\times \left(-\frac{3}{2} R^2 + \frac{1}{2} \sqrt{9R^4 + 12R^3 d} \right)^{-\frac{1}{2}} \times (9R^4 + 12R^3 d)^{-\frac{3}{2}}. \tag{25}$$

According to Eq. (21) and the chain's rule, the derivative of contact area/contact force to loading displacement can be expressed by:

$$\frac{\partial A_{ctc}}{\partial d} = \frac{\partial A_{ctc}}{\partial a_{ctc}} \times \frac{\partial a_{ctc}}{\partial \delta} = 2\pi a_{ctc} \times \frac{\partial a_{ctc}}{\partial \delta}, \tag{26}$$

$$\frac{\partial F_{ctc}}{\partial d} = \frac{\partial F_{ctc}}{\partial a_{ctc}} \times \frac{\partial a_{ctc}}{\partial d} = \left(\frac{4E^*}{R} a_{ctc}^2 + \frac{8E^*}{3R^3} a_{ctc}^4 \right) \times \frac{\partial a_{ctc}}{\partial d}, \tag{27}$$

$$\frac{\partial^2 F_{ctc}}{\partial d^2} = \left(\frac{8E^*}{R} a_{ctc} + \frac{32E^*}{3R^3} a_{ctc}^3 \right) \times \left(\frac{\partial a_{ctc}}{\partial d} \right)^2 +$$

$$+ \left(\frac{4E^*}{R} a_{ctc}^2 + \frac{8E^*}{3R^3} a_{ctc}^4 \right) \times \frac{\partial^2 a_{ctc}}{\partial d^2}. \tag{28}$$

Therefore, the adhesion force F_{ad}, real contact force F_s, and the real loading displacement d_s for the rigid spherical indentation model can be calculated according to Eqs. (21 – 28), which is still valid for high contact pressure.

3.2.2. Rigid sinusoidal indenter

As stated in Section 2.1, Hertz-like solution for sinusoidal asperity is only valid at small load, so it is necessary to get the accurate adhesion solution. The contact force can be written as a function of contact radius a_{atc}, which has the form:

$$F_{ctc} = \frac{2}{3} E^* \pi^2 \frac{h}{w^2} a_{ctc}^3 - \frac{4}{45} E^* \pi^4 \frac{h}{w^4} a_{ctc}^5. \tag{29}$$

According to chain's law, derivate contact area A_{ctc} to loading displacement d:

$$\frac{\partial A_{ctc}}{\partial d} = \frac{\partial A_{ctc}}{\partial a_{ctc}} \times \frac{\partial a_{ctc}}{\partial d} = 2\pi a_{ctc} \times \frac{\partial a_{ctc}}{\partial d}, \tag{30}$$

where: $\dfrac{\partial a_{ctc}}{\partial d}$ can be calculated by:

$$\frac{\partial a_{ctc}}{\partial d} = \frac{\sqrt{6}}{8\pi} \frac{w}{h} \left[\frac{3}{4} - \left(\frac{9}{16} - \frac{d}{2h} \right)^{\frac{1}{2}} \right]^{-\frac{1}{2}} \times \left(\frac{9}{16} - \frac{d}{2h} \right)^{-\frac{1}{2}}. \tag{31}$$

Continue deviating, we can obtain:

$$\frac{\partial^2 a_{ctc}}{\partial d^2} = \frac{\sqrt{6}}{8\pi} \frac{w}{h} \left\{ \left(-\frac{1}{8h} \right) \times \left[\frac{3}{4} - \left(\frac{9}{16} - \frac{d}{2h} \right)^{\frac{1}{2}} \right]^{-\frac{3}{2}} \times \left(\frac{9}{16} - \frac{d}{2h} \right)^{-1} + \frac{1}{4h} \times \left[\frac{3}{4} - \left(\frac{9}{16} - \frac{d}{2h} \right)^{\frac{1}{2}} \right]^{-\frac{1}{2}} \times \left(\frac{9}{16} - \frac{d}{2h} \right)^{-\frac{3}{2}} \right\}. \tag{32}$$

According to Eq. (29, 31, 32) and the chain's law,

$$\frac{\partial F_{ctc}}{\partial d} = \frac{\partial F_{ctc}}{\partial a_{ctc}} \times \frac{\partial a_{ctc}}{\partial d} =$$

$$= \left(2E^* \pi^2 \frac{h}{w^2} a_{ctc}^2 - \frac{4}{9} E^* \pi^4 \frac{h}{w^4} a_{ctc}^4 \right) \times \frac{\partial a_{ctc}}{\partial d}, \tag{33}$$

$$\frac{\partial^2 F_{ctc}}{\partial d^2} = \left(4E^* \pi^2 \frac{h}{w^2} a_{ctc} - \frac{16}{9} E^* \pi^4 \frac{h}{w^4} a_{ctc}^3 \right) \times \left(\frac{\partial a_{ctc}}{\partial d} \right)^2 +$$

$$+ \left(2E^* \pi^2 \frac{h}{w^2} a_{ctc}^2 - \frac{4}{9} E^* \pi^4 \frac{h}{w^4} a_{ctc}^4 \right) \times \frac{\partial^2 a_{ctc}}{\partial d^2}. \tag{34}$$

According to Eq. (13), the accurate loading interference becomes:

$$d_s = d - \frac{\left(4\gamma \pi a_{ctc} \times \dfrac{\partial a_{ctc}}{\partial d} \right)^{\frac{1}{2}}}{\left[\left(4E^* \pi^2 \dfrac{h}{w^2} a_{ctc} \dfrac{\partial a_{ctc}}{\partial d} - \dfrac{16}{9} E^* \pi^4 \dfrac{h}{w^4} a_{ctc}^3 \times \dfrac{\partial a_{ctc}}{\partial d} \right) \times \dfrac{\partial a_{ctc}}{\partial d} + \left(2E^* \pi^2 \dfrac{h}{w^2} a_{ctc}^2 - \dfrac{4}{9} E^* \pi^4 \dfrac{h}{w^4} a_{ctc}^4 \right) \times \dfrac{\partial^2 a_{ctc}}{\partial d^2} \right]^{\frac{1}{2}}}. \tag{35}$$

When considering adhesion, the real contact force and the adhesion force can be expressed in the following

forms:

$$F_s = 4\sqrt{6}E^* \frac{hw}{\pi}\left(\frac{3}{4}-\sqrt{\frac{9}{16}-\frac{1}{2}\frac{d}{h}}\right)^{\frac{3}{2}} - \frac{16}{5}\sqrt{6}E^* \frac{hw}{\pi}\left(\frac{3}{4}-\sqrt{\frac{9}{16}-\frac{1}{2}\frac{d}{h}}\right)^{\frac{5}{2}} + F_{ad}, \tag{36}$$

$$F_{ad} = -\frac{\partial F_{ctc}}{\partial d}\sqrt{2\gamma \times \frac{\partial A_{ctc}/\partial d}{\partial^2 F_{ctc}/\partial d^2}} = -\left(2E^*\pi^2\frac{h}{w^2}a_{ctc}^2 - \frac{4}{9}E^*\pi^4\frac{h}{w^4}a_{ctc}^4\right)\times\frac{\partial a_{ctc}}{\partial d}\times\sqrt{2\gamma\times\frac{\partial A_{ctc}/\partial d}{\partial^2 F_{ctc}/\partial d^2}}. \tag{37}$$

3.2.3. Rigid cone-shaped indenter

Similar with the above analysis, according to Eqs. (11) and (12), the derivation is relatively simple for rigid cone-shaped indenter. When considering adhesion, the real loading displacement and the real contact force can be expressed by:

$$d_s = d - \sqrt{2\gamma \times \frac{\partial A_{ctc}/\partial d}{\partial^2 F_{ctc}/\partial d^2}} = d - \sqrt{\frac{4\gamma}{E^* \tan\theta}d}, \tag{38}$$

$$F_s = F_{ctc} + F_{ad} = \frac{2}{\pi}E^*\frac{d^2}{\tan\theta} - \frac{8\left(E^*\right)^{\frac{1}{2}}\gamma^{\frac{1}{2}}}{\pi\left(\tan\theta\right)^{\frac{3}{2}}}d^{\frac{3}{2}}, \tag{39}$$

which is another explicit form, but the same as Chapter 6 in Ref. 25.

3.3. Results and discussion

In this section, we compare our model with the tradition theory by presenting the relationship between contact force, contact area and loading displacement. The influence of indenter shapes on contact responses is analyzed with consideration of adhesion as well. In present research, parameters of material property are taken as follows: the Young's modulus is taken to be 250 GPa and the Possion's ratio is taken to be 0.3. According to the material properties of polyethylene polyoxymethlene (POM) [27], the surface energy is taken to be 250 mJ/mm^2. When the surface energy is ignored, that is, the surface energy is taken to be $\gamma = 0$, the theoretical solution degrades to the basic Hertz or extended Hertz solution. Generally, the ratio of amplitude–to–wavelength h/λ has been restricted to $0.01<h/\lambda<3$, which covers most of the asperity shapes in realistic engineering surface [28].

For the rigid sinusoidal indentation model, the contact force and the contact area can be normalized through $F^*=F_s/(E^*h\lambda)$ and $A^*=A_s/\lambda^2$ to eliminate the asperity geometry effect. It can be seen from Fig. 3, a that when the adhesion force is not taken into consideration, the Hertz solution and the extended Hertz solution agree well with each other at small load level, but they gradually deviate with the increase of deformation. Using the extended-Hertz solution for this indentation model yields a slightly larger contact force for the same loading displacement. When the adhesion force is considered, the force will be negative when the load is small, as shown in the insert of Fig. 3, a. This is because the adhesion force exists: even if no extra load is applied, there exists a gravitational force between the interfaces. So, when loading is small, a pull-off zone exists, that is, the interface is in the tensile state. This is consistent with the phenomenon shown in Fig. 3, b. Differ-

ent from the Fig. 3, a, if adhesion is not considered, when the rigid indenter penetrates into the elastic substrate completely (complete contact), that is, the dimensionless loading displacement $d=h$, the deviation of contact area predicted by Hertz solution and extended Hertz solution is up to 33% (as shown by the dotted line in Fig. 3, b. Based on this, when adhesion force is taken into account, the contact area predicted by our model and JKR model will also have a large deviation under the condition of full contact, as shown by the solid line in Fig. 3, b. This directly leads to the difference of contact force contact area prediction, and

a

b
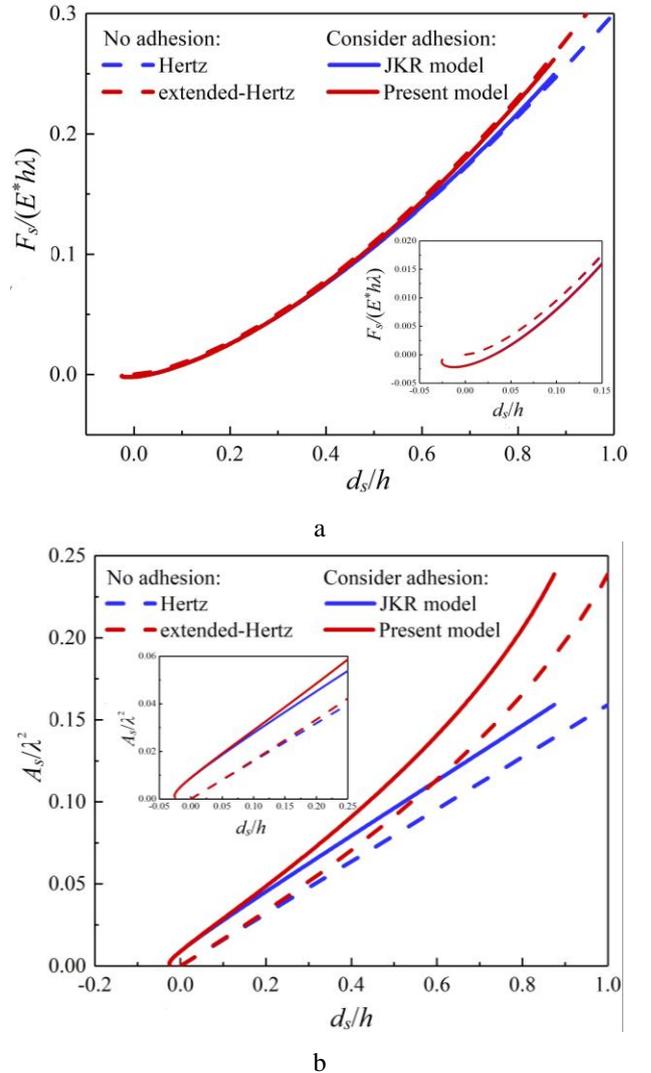
Fig. 3 Comparison with traditional Hertz model and JKR model when using extended-Hertz solution on non-adhesive and adhesive models (dash lines and solid lines, respectively): a) force versus loading displacement; b) area versus loading displacement; c) force-area relationship. The inserts show the pull-off zone in the case of small loading conditions

c
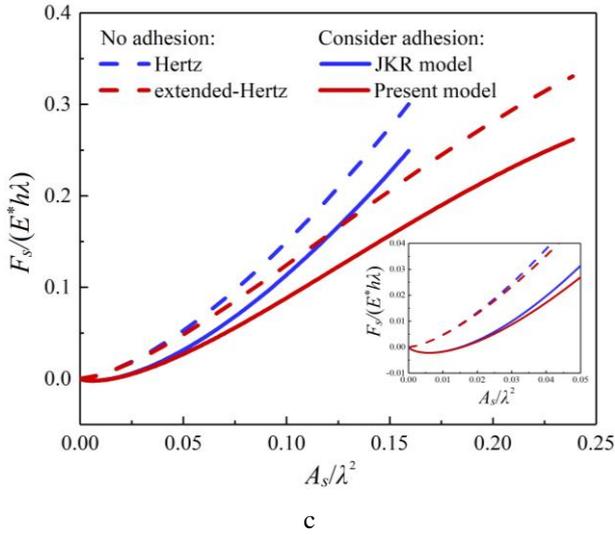
Fig. 3 Continuation

this relationship is one of the most concerned problems in the research field of contact mechanics. This again emphasizes the significance of exactly describing the gap profile. It will be more accurate to use the extended-Hertz solution to predict adhesion effect and the rough surface analysis.

Different from the Fig. 3, a, if adhesion is not considered, when the rigid indenter penetrates into the elastic substrate completely (complete contact), that is, the dimensionless loading displacement $d=h$, the deviation of contact area predicted by Hertz solution and extended Hertz solution is up to 33% (as shown by the dotted line in Fig. 3, b. Based on this, when adhesion force is considered, the contact area predicted by our model and JKR model will also have a large deviation under the condition of full contact, as shown by the solid line in Fig. 3, b. This directly leads to the difference of contact force contact area prediction, and this relationship is one of the most concerned problems in the research field of contact mechanics. This again emphasizes the significance of exactly describing the gap profile. It will be more accurate to use the extended-Hertz solution to predict adhesion effect and the rough surface analysis.

Different from the spherical indenter with a fixed curvature radius, the sinusoidal indenter and the cone-shaped indenter have different combinations of aspect ratio (h/λ or h/w), which can characterize the rough surface in detail. For a single indentation model, different profiles affect the contact relationships significantly. It can be seen in Fig. 4, a that the maximum negative force value (maximum pull-off force) increases with the decrease of aspect ratio. This is because a larger force is required when pulling the smoother surface apart. This result is consistent with Fig. 4, b. Fig. 4, b shows that the influence of indenter shapes on the area-loading displacement relationship is more significant. This again emphasizes that the adhesion effect affects the whole contact response mainly through the area displacement relationship. If adhesion is not taken into consideration, the contact response coincides with each other even if the profile changes, as shown by the solid line in Fig. 4, c, but the asperity shape affects the contact responses greatly when adhesion is considered. The influence of the adhesive force on the contact response increases with the decrease of the asperity ratio h/λ. This is because the smoothness of the surface decreases as the

ratio h/λ decreases. Adhesive contact is more easily to occur for smooth surfaces, just as contact between glasses. For cone-shaped indenter, the influence of adhesion force on the force versus loading displacement relationship can be ignored, and the contact relationship is still affected by the area displacement relationship, as shown in Figs. 4, d- and 4, e. Unlike the sinusoidal indenter, there is no obvious pull-out zone for the conical indenter model when taking adhesion into consideration, as shown in Figs. 4, d-f. The force area relationship in Fig. 4, f is nearly linear, which means that the contact response is more easily to be predicted by analytical method, and it is easier to be used in engineering. When the value of adhesion force equals to the force predicted by extended-Hertz solution, the contact radius in self-equilibrium status can be obtained. In this case, the objects will stick together due to the action of adhesion force, resulting in extrusion deformation, even if no external load is applied. When $\partial\left(F_{ctc} - F_{ad}\right)/\partial a_{ctc} = 0$,

a

b
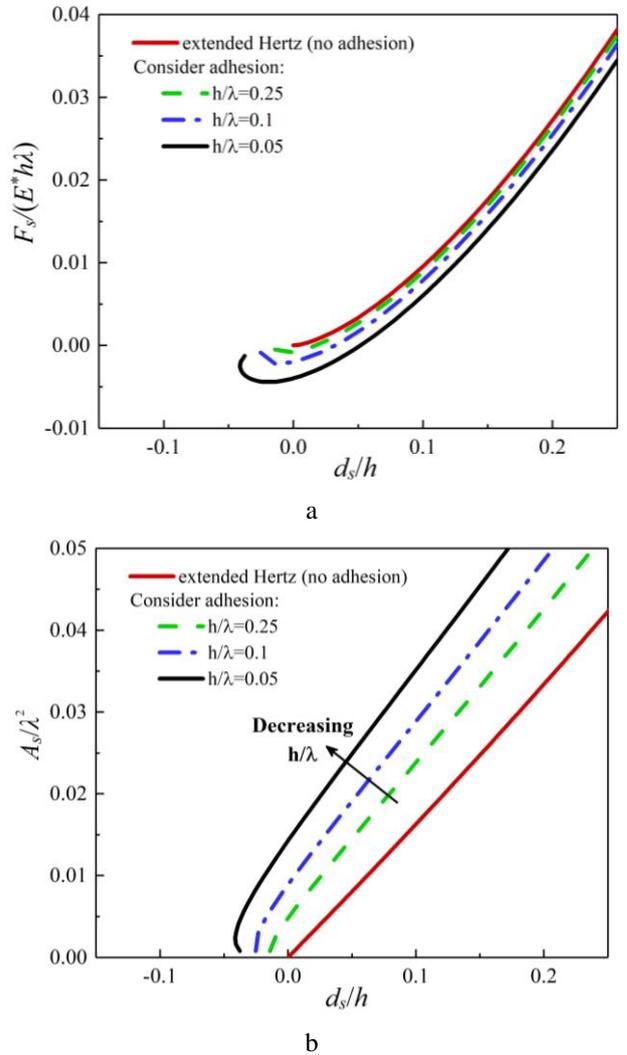
Fig. 4 The contact and adhesive responses of different profiles of indenters: For sinusoidal indenter, a) dimensionless force versus loading displacement relationship; b) dimensionless area versus loading displacement relationship; c) dimensionless force versus area relationship. For cone-shaped indenter, d) dimensionless force versus loading displacement relationship; e) dimensionless area versus loading displacement relationship; f) dimensionless force versus area relationship

c

d

e

f
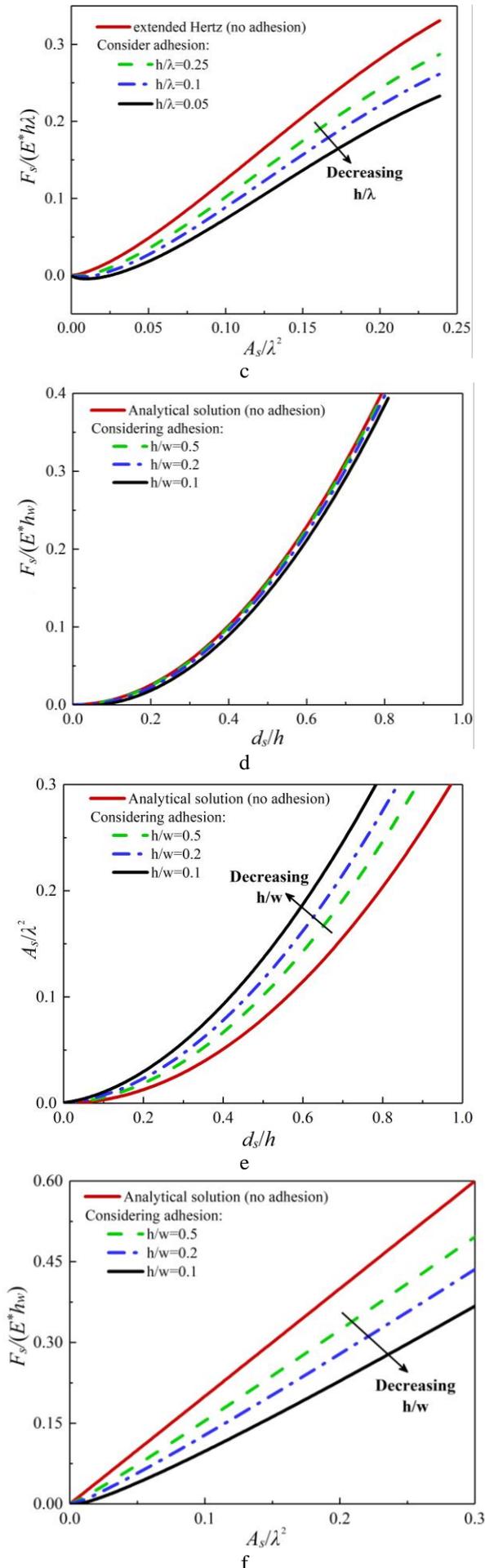
Fig. 4 Continuation

the system is in a critical state of minimum energy. When the force is at the minimum value (maximum negative value), it represents the pull off force, representing the minimum force needed to separate the two objects, which is a very important physical quantity. The corresponding contact radius is critical contact radius, which can be investigated easily in experiments. It is worth noting that as an improved model of spherical indenter (sinusoidal profile indenter), an obvious pull-off zone exists, and the force-area relationship is non-linear, as shown in Figs. 4, a-c. But the pull-off zone does not exist in the adhesive behaviors of cone-shaped indenter, and the force versus area relationship behaves linearly, as shown in Figs. 4, d-f.

4. Application to rough surface contact

In Section 3, we presented the consequence of using adhesion theroy based on extended-Hertz solution to describe the mechanical response of a single asperity. In this section, we focus on the consequences of using the proposed adhesive solution for multi-sinusoidal/cone-shaped indenters in contact with an elastic substrate. The modeling of contact between two rough surfaces is usually simplified by a flat surface and a rough surface: one of them is rigid, and the other is deformable. In the previous studies, some rough surface models considered flattening (a rigid flat in contact with a deformable rough surface), while others considered indentation (a rigid rough surface in contact with a deformable substrate). For example, Kogut and Etsion [29] simplified the contact problem into the flattening of the deformable rough surface (flatening problem), while Yin and Komvopoulos [30] investigated a rigid rough surface penetrated into a flat substrate (indentation problem). In present section, we model the discrete indentation model by assuming that the rigid rough surface is composed of a series of indenters, which is in contact with a soft elastic substrate.

The contact of the surface is analyzed through discrete GW modeling: a typical approch for modeling rough surfaces, whose height follows a Gaussian distribution with the average value $AVG(h)$ and standard deviation σ. We assume that all summits have the same base width λ, but different heights. If the individual summit come into contact with the soft substrate, it keeps in contact from now on. We define the surface roughness parameter as $\beta = \sigma/AVG(h)$, i.e., the ratio between standard deviation and average of the Gaussian distribution. In fact, according to Section 3.2, the aspect ratio h/λ is also a parameter to characterize surface roughness. Fig. 5 shows a simple schematic of this model：the heights of the rigid rough surface follow Gaussian distribution. The dash and solid line represent the initial and present position, respectively. Since the rough surface is rigid, it will not
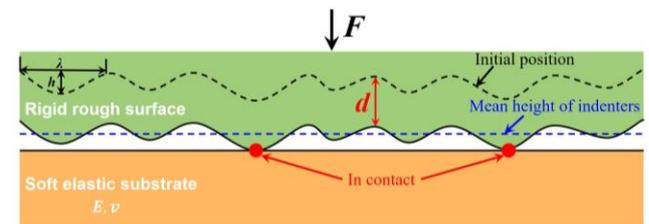
Fig. 5 Schematic of the problem: the rigid wavy surface is in contact with a soft elastic substrate

deform during the loading process. The contact force and area can be calculated by $F = \sum_{i=1}^{N} F_i, A = \sum_{i=1}^{N} A_i$, where F_i and A_i are the contact force and the contact area of each single indenter i, and they can be calculated according to Section 2 and 3.

The influence of randomness decreases as the number of asperities increases, ultimately recovering a Gaussian distribution in terms of heights. In present study, the total number of asperities is chosen to be $N = 10000$ in the discrete GW model, which is the minimum value of eliminating influence of random parameters. For a rough surface which is composed of sinusoidal asperities and conical asperities (with the same average roughness), shows the contact response of surfaces with different roughness and different surface energy can be seen from Fig. 6. Fig. 6, a compares the force versus loading displacement relationship of rough surface with different roughness parameters. The dash lines represent the results when adhesion is not considered, while the solid lines represent the adhesive results. It should be noted that although our program is valid for complete contact, Fig. 6, a only shows the contact relationships when the dimensionless loading displacement is no more than 0.2 h. This is due to the completely different behaviour of adhesion effect at the initial stage of loading process, which needs to be paid special attention. Different from the non-adhesive discrete model, the force versus loading displacement relationship for the discrete model considering adhesion does not increase monotonically, but decreases at first and then
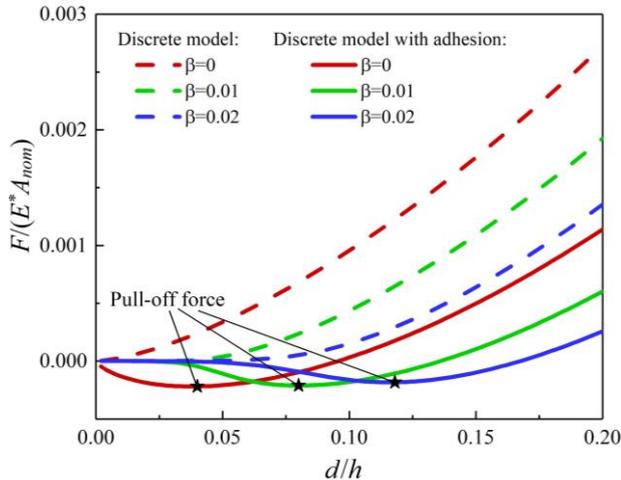
a
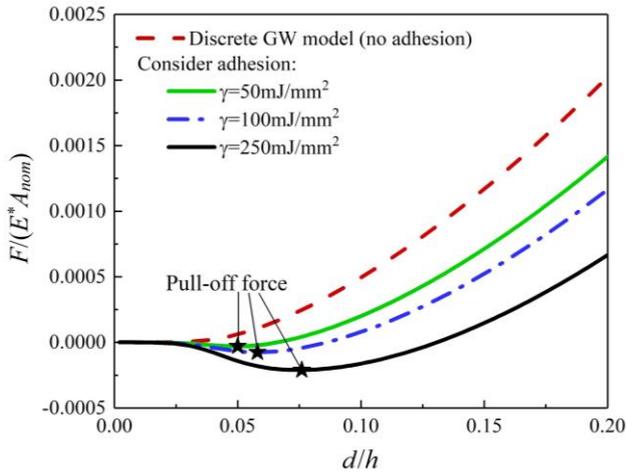
b
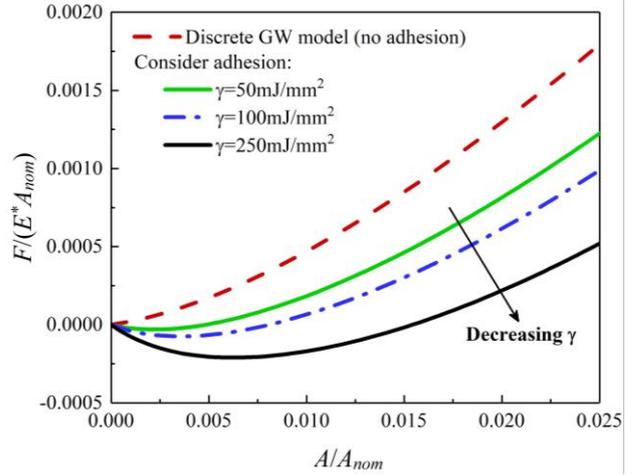
c
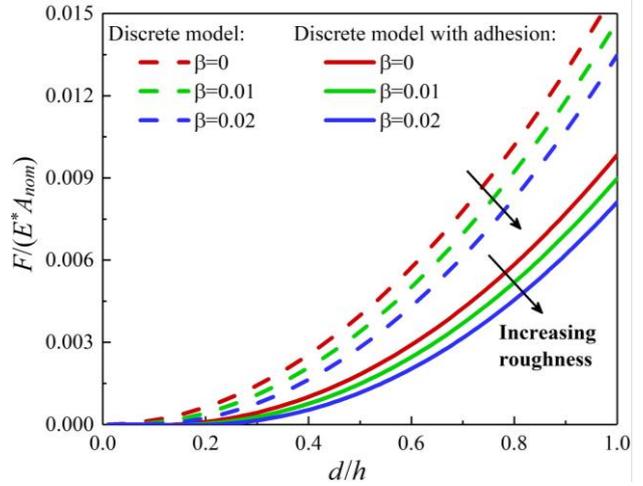
d

Fig. 6 Comparison of discrete GW model without adhesion and adhesive rough surface model with different surface roughness and surface energy: a) dimensionless force versus loading displacement relationship with different surface roughness for rough surface composed of sinusoidal indenters; b) dimensionless force versus loading displacement relationship with different surface energy for rough surface composed of sinusoidal indenters (the scatters represent the pull-off force); c) dimensionless force versus area relationship with different surface energy for rough surface composed of sinusoidal indenters; d) dimensionless force versus loading displacement relationship with different surface roughness for rough surface composed of cone-shaped indenters; e) dimensionless force versus loading displacement relationship with different surface energy for rough surface composed of cone-shaped indenters; f) dimensionless force versus area relationship with different surface energy for rough surface composed of cone-shaped indenters

e

f
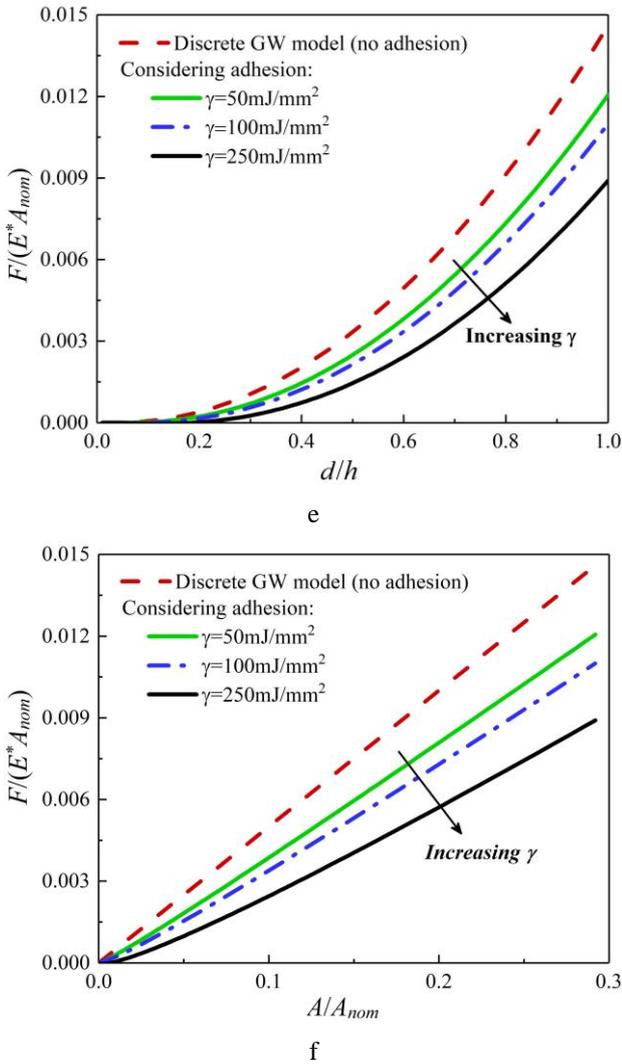
Fig. 6 Continuation

increases. This is because a pull-off zone exists in rough surface analysis, which is similar with single indentation model in Section 3. Fig. 6, b shows the contact responses of rough surface with different surface energy. The value of critical pull-off force increases with the increasing of surface energy. The state of pull-off force is a critical equilibrium state, which is denoted by the scatters. This is also consistent with the result in Fig. 6, c. The nonmonotonicity of the dimensionless force-area curve shows that it is more difficult to pull the two surfaces apart when surface energy is larger. Unlike the above results, for rigid rough surface with cone-shaped indenters, the effect of roughness on contact response is not obvious, as shown in Fig. 6, d. The pull-off zone does not exist, which means it is easier to separate the two surfaces. With the decreasing of surface energy, the contact response tends to approach the contact response predicted by discrete GW model without consideration of adhesion, as shown in Fig. 6, e. Different from the results in Fig. 6, c, Fig. 6, f shows that the dimensionless force versus area relationship is generally linear, which is convenient to predict contact relationships in engineering. Generally speaking, surface roughness can greatly reduce the adhesion between solids, and the surface energy has great influence on the contact response. It tends to be closer to non-sticky contact with the decreasing of surface energy, and the critical equilibrium state changes

with the asperity profile, surface roughness, and surface energy.

5. Conclusion

The adhesion behaviour between interfaces is widely investigated in engineering and scientific research. However, due to the complexity of the loading conditions and the surface topography, the traditional adhesion theories such as JKR theory, cannot capture the adhesion effect between surfaces. In order to better understand the adhesion behavior between contact surfaces, we investigated the adhesive responses according to the improved elastic analytical solutions for single indenter. Based on this, we further studied the adhesive responses of rough surface modelling as well. It provides a theoretical basis for predicting the contact response between surfaces when the adhesion force is considered. The conclusions of the present study are:

1. According to the accurate description of the contact region, an analytical solution is first derived for rigid indenters in contact with an elastic soft substrate, which is still valid for complete contact. For spherical and sinusoidal indenter, the analysis is based on Steuermann solution, while for cone-shaped indenter, the analysis is based on method of dimensionality reduction. These analytical solutions are the theoretical basis of adhesive contact modeling and rough surface analysis later.

2. Except spherical indenter under small strain condition, the commonly used Hertz solution and the conventional JKR theory cannot be directly used for other profiles of indenters and near complete contact. Based on the elastic responses for near complete contact, the adhesive effect is then taken into consideration in the frame of JKR theory, and accurate analytical solutions are provided for different shapes of indenters. The results show that there exists an obvious pull-off zone for sinusoid-shaped indenter, but there is no such zone for cone-shaped indenter, indicating that adhesion is more easily to happen for smooth and geometrically continuous surfaces.

3. In addition to the above theory which is based on single indentation model to describe the adhesion phenomenon, a multi-asperities model is also proposed to describe the adhesion behaviour between rough surfaces. This provides a method for the investigation of adhesion properties of rough surfaces with complex morphologies. The results show that both surface roughness and surface energy affect the adhesion and contact properties of rough surfaces. Surface roughness can be characterized by two parameters (individual indenter profile and random distribution parameter). With the increasing of surface roughness, the adhesion force will be greatly reduced. The contact response will be closer to non-adhesive contact with the decreasing of surface energy.

Appendix: Analytical and FEM solutions of cone-shaped indenter

For the contact problem between a cone and an elastic half-space (Fig. 1, c), the reduction method can be used to calculate the contact radius and the normal force as a function of the indentation depth.

According to the Method of Dimensionality Reduction proposed by Popov 25, 26] the form of the cone

can be described by the equation $f(r) = tan\theta \cdot r$, and the one-dimensional profile is given by $g(x)=(\pi/2)tan\theta\cdot|x|$. According to the geometry relationship of the contact region in Fig. 1, d, the deformation of the substrate can be expressed by:

$$u_z(x) = d - \frac{\pi}{2} \cdot tan\theta \cdot |x|, \tag{40}$$

where: $u_z(a) = 0$, at the boundary of the contact region. Therefore, the contact radius is the function of loading displacement, which has the form:

$$a = \frac{2}{\pi} \cdot \frac{d}{tan\theta}. \tag{41}$$

The normal force is obtained by Eq. (42) (see Eq. (3.10) in Ref. [26]).

$$F_N = 2E^* \int_0^a u_z(x)dx =$$
$$= 2E^* \int_0^a \left(d - \frac{\pi}{2} x \tan\theta \right) dx = \frac{2}{\pi} E^* \frac{d^2}{\tan\theta}. \tag{42}$$

Fig. 7, a shows an example of the employed mesh of the cone-shaped indentation model. The contact response obtained by FEM simulation corresponds well with the analytical solution (Eq. (38)), indicating that the analytical solution is still valid for complete contact.

a

b
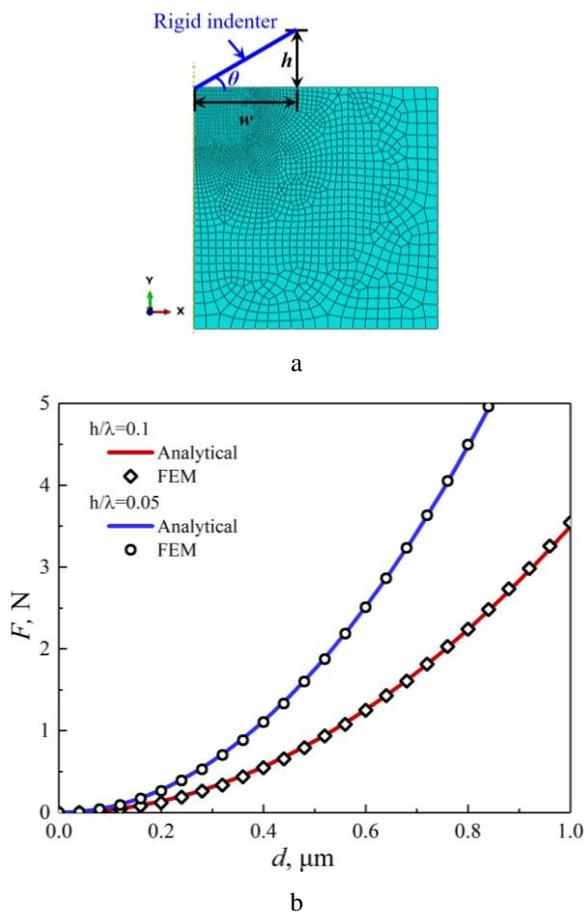
Fig. 7 (a) Axisymmetric mesh example for the cone-shaped indentation model; (b) comparison of the analytical solution and FEM results

Reference

1. **Zhao, Y. P.; Wang, L. S.; Yu, T. X.** 2003. Mechanics of adhesion in MEMS – a review, Journal of Adhesion Science and Technology 4: 519-546. https://doi.org/10.1163/15685610360554393.
2. **Tayebi, N.; Polycarpou, A. A.** 2005. Reducing the effects of adhesion and friction in micro electromechanical systems (MEMs) through surface roughening: Comparison between theory and experiments, Journal of Applied Physics 98: 357. https://doi.org/10.1063/1.2058178.
3. **Autumn, K; Liang, Y. A.; Hsieh, S. T.; Zesch, W; Chan, W. P.; Kenny, T. W.; Fearing, R.; Full, R. J.** 2000. Adhesion forces of a single gecko foot-hair, Nature 405: 681-685. https://doi.org/10.1038/35015073.
4. **Autumn, K.; Sitti, M.; Liang, Y. A.; Peattie, A. M.; Hansen, W. R.; Sponberg, S.; Kenny T. W.; Fearing, R.; Israelachvil, J. N.; Full, R. J.** 2002. Evidence for van der Wals adhesion in gecko seta, Proceedings of the National Academy of Sciences 99: 12252-12256. https://doi.org/10.1073/pnas.192252799.
5. **Yao, H.; Gao, H.** 2006. Mechanics of robust and releasable adhesion in biology: Bottom-up designed hierarchical structures of gecko, Journal of the Mechanics and Physics of Solids 54: 1120-1146. https://doi.org/10.1016/j.jmps.2006.01.002.
6. **Johnson, K. L.; Kendall, K.; Roberts, A. D**. 1971. Surface energy and the contact of elastic solids, Proceedings of Royal of Society 324:1558. https://doi.org/10.1098/rspa.1971.0141.
7. **Derjaguin, B. V.; Muller, V. M.; Toporov, Y. P**. 1975. Effect of Contact Deformations on the Adhesion of Particles, Journal of Colloid and Interface Science 53: 314-326. https://doi.org/10.1016/0021-9797(75)90018-1.
8. **Ciavarella, M**. 2017. On the use of DMT approximations in adhesive contacts, with remarks on random rough contacts, Tribology International 114: 445-449. https://doi.org/10.1016/j.triboint.2017.04.046.
9. **Tabor, D**. 1977. Surface forces and surface interactions, Journal of Colloid and Interface Science 58: 2–13. https://doi.org/10.1016/0021-9797(77)90366-6.
10. **Ciavarella, M**. 2018. An approximate JKR solution for a general contact, including rough contacts, Journal of the Mechanics and Physics of Solids 114: 209-218. https://doi.org/10.1016/j.jmps.2018.03.005.
11. **Polina, P.; Perni, S**. 2011. Comparison of JKR- and DMT-based multi-asperity adhesion model: Theory and experiment, Colloids and Surfaces A Physicochemical and Engineering Aspects 383: 95-101. https://doi.org/10.1016/j.colsurfa.2011.01.011.
12. **Hui, C. Y.; Liu, T.; Salez, T.; Raphael, E.; Jagota, A.** 2015. Indentation of a Rigid Sphere into an Elastic Substrate with Surface Tension and Adhesion, Proceedings of Royal Society A 471: 2175. https://doi.org/10.1098/rspa.2014.0727.
13. **Zhang, L.; Ru, C. Q**. 2019. A refined JKR model for adhesion of a rigid sphere on a soft elastic substrate, Journal of Applied Mechanics 86: 051004. https://doi.org/10.1115/1.4042574.
14. **Johnson, K. L**. 1995. The adhesion of two elastic bod-

ies with slightly wavy surfaces, International Journal of Solids and Structures 32: 423-430.
https://doi.org/10.1016/0020-7683(94)00111-9.

15. **Perni S.; Prokopovich, P**. 2015. Multi-asperity elliptical JKR model for adhesion of a surface with non-axially symmetric asperities, Tribology International 88: 107-114.
https://doi.org/10.1109/LEOS.2001.968954.

16. **Sohn, D.; Won, H. S.; Jang, B.;** et al. 2015. Extended JKR theory on adhesive contact between elastic coatings on rigid cylinders under plane strain, International Journal of Solids and Structures 71:244-254.
http://doi.org/10.1016/j.ijsolstr.2016.03.024.

17. **Popov, V. L.; Pohrt, R.; Li, Q**. 2017. Strength of adhesive contacts: Influence of contact geometry and material gradients, Friction 5: 308-325.
http://doi.org/10.1007/s40544-017-0177-3.

18. **Poon, C. Y.; Bhushan, B**. 1995. Comparison of surface roughness measurements by stylus profiler, AFM and non-contact optical profiler, Wear 190:76–88.
http://doi.org/10.1016/0043-1648(95)06697-7.

19. **Jourani, A**. 2015. New 3D numerical model of rough contact: influence of mode of surface deformation on real area of contact and pressure distribution, Journal of Tribology 137: 011401.
http://doi.org/10.1115/1.4028286.

20. Fischer-Cripps AC. Nanoindentation. New York: Spring-Verlag: 2002.

21. **Ciavarella, M**. 2018. A very simple estimate of adhesion of hard solids with rough surfaces based on a bearing area model, Meccanica.
http://doi.org/10.1007/s11012-017-0701-6.

22. **Ciavarella, M**. 2015. Adhesive rough contacts near complete contact, International Journal of Mechanical Sciences 104:104-111.
http://doi.org/10.1016/j.ijmecsci.2015.10.005.

23. **Johnson, K. L**. Contact Mechanics. Cambridge, UK: Cambridge University Press; 1985.

24. **Zhang, S.; Song, H.; Sandfied, S.; Liu, X.; Wei, Y. G.** 2019. Discrete Greenwood–Williamson modeling of rough surface contact accounting for three-dimensional sinusoidal asperities and asperity interaction, Journal of Tribology 141:121401.
http://doi.org/10.1115/1.4044635.

25. **Popov, V. L**. 2010. Contact Mechanics and Friction.

26. **Popov, V. L**. 2016. Hess M. Method of Dimensionality Reduction in Contact Mechanics and Friction.

27. **Wu, K. C.; You, H. I**. 2007. Determination of solid material elastic modulus and surface energy based on JKR contact model, Applied Surface Science 253:

8530-8537.
http://doi.org/10.1016/j.apsusc.2007.04.037.

28. **Gao, Y. F.; Bower, A. F.; Kim, K. S.; Lev, L.; Cheng Y. T**. 2006. The behavior of an elastic–perfectly plastic sinusoidal surface under contact loading, Wear 261: 145–154.
http://doi.org/10.1016/j.wear.2005.09.016.

29. **Kogut, L.; Etsion, I**. 2002. Elastic-plastic contact analysis of a sphere and a rigid flat, Journal of Applied Mechanics 69: 657–662.
http://doi.org/10.1115/1.1490373.

30. **Yin, X.; Komvopoulos, K**. 2012. A discrete dislocation plasticity analysis of a single-crystal semi-infinite medium indented by a rigid surface exhibiting multi-scale roughness, Philosophical Magazine 92: 2984–3005.
http://doi.org/10.1080/14786435.2012.682178.

Siyuan Zhang, Yanwei Liu

EFFECT OF SURFACE ADHESION ON THE ROUGH CONTACT RESPONSE NEAR COMPLETE CONTACT

S u m m a r y

The adhesion phenomena between interfaces are widely investigated in engineering and scientific research. Due to the complexity of loading condition and surface topography, the traditional adhesive theory has many limitations. To better understand the adhesive properties of rough surfaces, we release the restrictions of classical JKR theory and propose a new adhesive model for single asperity. Initiated by this, a discrete rough surface contact model is presented, which extends the application scope of the traditional theory. The results show that adhesion is more easily to happen for smooth and geometrically continuous surfaces. The overall adhesion effect will be reduced in rough surface analysis with the increasing of surface roughness and the decreasing of surface energy. Our research sheds light on the understanding of the adhesion between solids and provides a theoretical guidance for the design of adhesion biomimetic materials and MEMS systems.